JTTEE5 10:287-292

Estimation of Three-Dimensional Connectivity of Internal Defects in Coatings Using Fractal Analysis

N. Llorca-Isern, Gemma Bertran Vidal, J. Jorba, L. Bianchi, and D. Sánchez

(Submitted 16 March 2000; in revised form 22 August 2000)

The connectivity of a porous medium is an important topological characteristic, which indicates the extent to which internal defects (*e.g.*, porosity or micro/macrocracking) are connected. Up to now, connectivity has been studied by various stereological procedures based on the "net volume tangent counts" proposed by DeHoff and performed on pairs of consecutive sections of an interconnected structure. However, the drawbacks of these procedures are their use of invasive techniques and manual counting.

Connectivity is here studied with fractal geometry instead of conventional Euclidean geometry. The porosity network of a thermal spray sample may be fractal, and so can be at least partly characterized by fractal dimension. Modifications in connectivity could be reflected in changes in the fractal dimension. If changes in the connectivity, as characterized by changes in fractal dimension, can be adequately demonstrated by the computerized analysis of confocal scanning laser microscope (CSLM) images, then the technique may provide a useful, noninvasive way of improving the characterization of thermal spray coatings.

The study also seeks to show how connectivity differences affect the mechanical properties of the coating and whether fractal analysis is able to detect these changes in mechanical properties.

Keywords confocal microscopy, connectivity, fractal dimension, porosity, thermal spray coatings, three-dimensional characterization

1. Introduction

Ceramic thermal spray coatings have defects, pores, and cracks, which are inherent to the spraying technique. The size of these defects varies according to the specific technique used (considering controlled spraying parameters) and with the materials used as substrate-coating pair. Most applications require a degree of porosity in order to accommodate the ceramic subjected to thermal cycling. The defects originate mainly in the shrinkage that occurs when particles are rapidly cooled on the substrate. They are also a consequence of the different thermal expansion coefficients of substrate and coating materials. The weakest parts of these structures are the substrate-coating interface, especially for increasing differences between thermal expansion coefficients, and the interface between deposited particles due to the areas of little contact between them. The coating will fracture at one of these two zones.[1] A direct consequence of plasma spraying is the generation of residual stresses reflected in the final quality of the coating. These limit the adherence of coating and substrate, and decrease its mechanical properties. A compromise between the need for low porosity and the real number of defects makes it necessary to formulate an objective parameter to evaluate the amount of defects present in the coating.

Conventional characterization of thermal spray coatings produces optical and electron images as well as compositional and structural information. Confocal microscopy to study the interconnected defects network is a useful tool with minimum interaction between the sample and the technique. It allows three-dimensional information from a controlled volume of sample by optical sectioning to be acquired by the laser beam without any mechanical coating damage.[2–5] In the present study, the samples were impregnated with a low viscosity fluorescent resin and then observed with the confocal microscope under fluorescence and using the extended focus conditions. The images produced were then studied with respect to their fractal geometry.

Fractal geometry describes a great number of natural structures, which are irregular, rough, or fragmented. These irregularities are of different sizes but are related to each other because they show similar features when the observation scale is decreased. The main characteristic of any fractal object is its fractal dimension, D, a measurement of its degree of irregularity and interruption.[6–10] This measurement can be related to the connectivity of the system. There are several methods for determining the fractal dimension of an object. Although the resulting values are not the same, all of them confirm that increasing the fractal dimension increases the complexity of the structure.[6] In the present study, the Boulignan dimension method was used. This method is based on the box-counting process, defined as[7,8,10]

$$D_B = \lim_{e \to 0} - \frac{\mathrm{Ln}\ N(e)}{\mathrm{Ln}\ e} \qquad \text{(Eq 1)}$$

where e is the scale or dimension of the box, $N(e)$ the number of

N. Llorca-Isern and **Gemma Bertran Vidal,** Departament de E.Q.-Metal.lúrgia, Universitat de Barcelona, 08028 Barcelona, Spain. **L. Bianchi,** CEA LR-BP 16-37260 MONTS– France. **J. Jorba and D. Sánchez,** Departament Mecànica, Aplicada, EUETI-UPC. Comte d' Urgell 187, 08036 Barcelona, Spain. Contact e-mail: llorca@material.qui.ub.es.

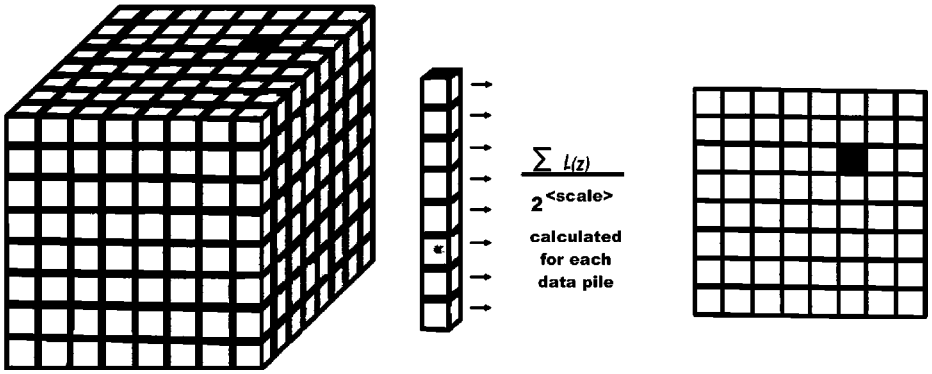

Fig. 1 Schematic representation of the extended focus mode for the confocal microscope

Table 1 Sample codification

	Medium temperature		Highest velocity	
Substrate	**Highest velocity**	**Lowest velocity**	**Lowest temperature**	**Highest temperature**
Aluminum (a)	1a	2a	3a	4a
Steel (i)	1i	2i	3i	4i

cells needed to define the figure to be studied, and D_B the Bouligand dimension.

In this equation, the growth of $N(e)$ shows the level of irregularity of the set under observation, whether planar or volumetric, when examined with an e scale.

2. Experimental Methodology

2.1 Materials

Plasma-sprayed ZrO_2-Y_2O_3 coatings were sprayed on steel (identified as *i*) and on aluminum (identified as *a*) substrates. In order to generate different microstructures, the relative velocity of the torch substrate and the substrate temperature were varied.[11] Samples coded as 1 represent the highest velocity and samples coded as 2 are for the lowest velocity, both at medium temperature. Samples coded as 3 are of the lowest temperature and samples coded as 4 are of the highest temperature and highest relative velocity (Table 1).

The coatings were impregnated with the epoxy resin Spurr (Sigma, St. Louis, MO) containing fluorescent particles (Epodye, Struers (Rodovre, Denmark)) for studying the different penetration levels. The sample preparation is reported elsewhere.[12]

2.2 Confocal Microscopy

Optical sections from different focal planes are combined to find information of a known volume of the sample. The laser scans only a focal plane of the sample, discriminating against out-of-plane information. In our case, the fluorescent intensity is the recorded information. This operation is repeated for a number of planes selected by the user inside the sample. The depth from which information will be taken depends on the resolution of the equipment. The information from the different focal planes is then processed and its recombination produces a reconstructed image showing the features of the selected volume of the sample.

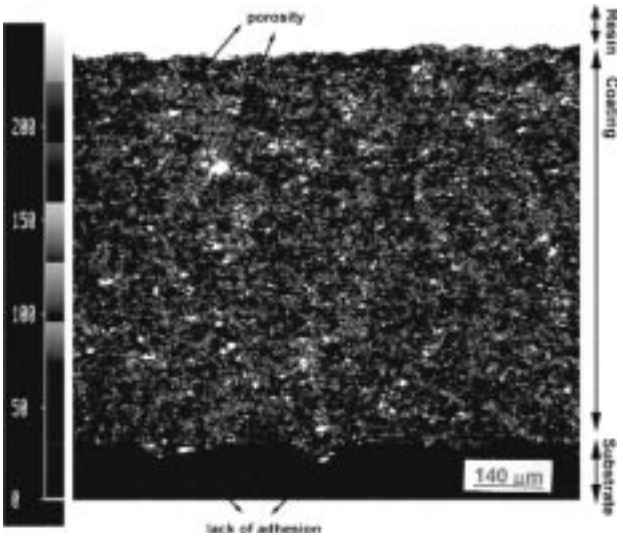

Fig. 2 Three-dimensional reconstruction of a plasma sprayed zone. An extended focus image was created with a contrast-optimized average projection of 20 *x-y* optical sections, 5.26 μm apart. The volume under observation is 998.4 × 998.4 × 56.2 μm^3. Scale bar indicates 140 μm

The operating method of extended focus in the confocal microscope is based on the addition of all the gray values shown by the pixels occupying the same position; this procedure is performed for each image to build up the final reconstruction. The extended focus allows the observation of large areas and depths, which makes the depth of field very large in a single image[4,5] (Fig. 1).

An example of the image obtained with the extended focus mode is shown in Fig. 2, in which the coating, the substrate-coating interface, and the substrate (bottom part of the micrograph) can be resolved. The bright spots are saturation points at which fluorescence is very intense and correspond to the fluorescence accumulation zones of the samples.

2.3. Experimental Estimation of the Fractal Dimension

The Boulignan equation (Eq 1) enables a numerical algorithm for measuring the fractal dimension to be constructed. Experimentally, the fractal dimension is measured following the Boulignan equation, which consists of the calculation of the slope of the log of the measured area in front of the log of the measurement tool.

If we consider E as the set of points to be studied, we have to choose e_1 and measure its $Ne_1(E)$. This value can be found by direct counting (if we are measuring its area by the box-counting method) or from any other property that changes with the observation scale and can be measured easily. Next, another e_2 is chosen and its $Ne_2(E)$ measured and so on with the other points of the set. Finally, all the values are represented as logarithm $Ne_k(E)$ versus logarithm e_k. The fractal dimension corresponds to the slope of the linear part of the asymptotic representation obtained. For physical systems modeled by fractals, the scale e depends on the tool measurement resolution for establishing its working detection range, and also on the physical meaning of the scale itself relative to the studied system.[10]

2.4 Image Analysis

The surfaces with fractal characteristics show a mathematically infinite area, which means that this area increases as the scale becomes finer. In the present study, fractal dimension was calculated with gray-level intensity as the measurement tool. The gray levels define the image's fluorescence intensity, which corresponds to porosity and other connected defects of the system and is, therefore, an intrinsic characteristic of the microstructure. Therefore, a bigger pore contains more accumulated fluorocrom and, consequently, fluoresces more. In addition, the higher the interconnected network of defects, the more this shows up through fluorescence intensity. With this information, an algorithm measuring the fractal dimension of the images obtained using the confocal microscope is proposed. The image's gray level as a function of the relative pixel size used in the measurement is counted.

A matrix representing the intensity levels of each pixel in an identically divided 255 scale is built up from the digital images. These intensity values are used by the program to calculate the logarithm of the surface, which is the property of the structure, the variation of which, depending on the observation scale, will provide the structure's fractal dimension. The surface is measured by taking the pixel size together with its gray level. From these values, the representation of the logarithm surface versus logarithm cell size will provide the slope (b in Eq 2), which is added to the Euclidean dimension (a in Eq 2) to obtain the fractal dimension (D in Eq 2):

$$D = a + b \quad \text{(Eq 2)}$$

The first step in cell analysis is to build up the cell's surface with the proposed algorithm. For this, the intensity of the four vertices of the cell and their mean value are represented in an X-Y intensity diagram. The union of these intensity points (each two vertices with the mean value) will produce four new surfaces. The sum of the resulting areas is the fractal surface and is one point in the logarithm-logarithm representation (Fig. 3). By enlarging the cell size, details are lost and the surface to be measured decreases. The number of points to count, which is the number of measurements shown, depends on the image resolution.

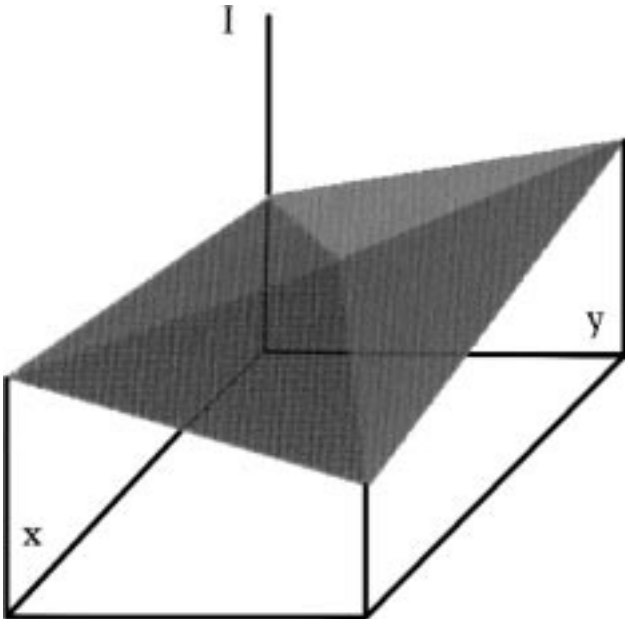

Fig. 3 Construction of the fractal surface for an individual cell. X and Y are the cell sizes (in pixels), and I is the fluorescence intensity

The present algorithm is different from others suggested in the bibliography in the way in which the image is divided to obtain the specific surface, which is used for determining the fractal dimension of the system.

3. Results and Discussion

3.1 Fluorescent Intensity and Defects Distribution

The microstructure is evaluated with the images obtained by the confocal microscope in its extended focus mode. Each image is the reconstruction of different sections (focal planes), and each pixel used for the calculation is the sum of the fluorescence intensities of each pixel occupying the same position in all the sections, which are combined to form the final image (Fig. 1). Figure 2 is a reconstructed image in extended focus. The density of fluorescence and its distribution is clearly seen. From this information, some parameters can be stabilized and used for comparison purposes, as, for example, penetration of the resin, microfracture orientation, and adhesion/cohesion of the coating.

Preliminary work was performed to achieve the optimal image conditions for the study. It was observed that maximum saturated areas were detrimental to the calculation, and so the laser potential and other internal parameters of the microscope were adjusted to avoid maximum saturated areas. All the samples were observed and the images taken under the same conditions.

Results are plotted as logarithm surface versus logarithm number of steps. The program enables the interval between steps

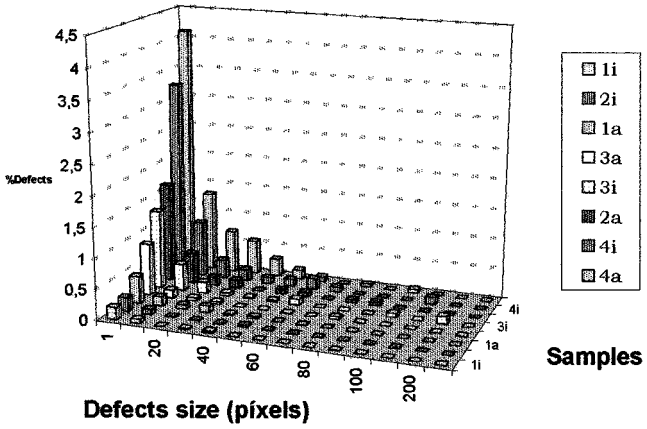

Fig. 4 Percentage of defects for the samples as a function of the pixel size

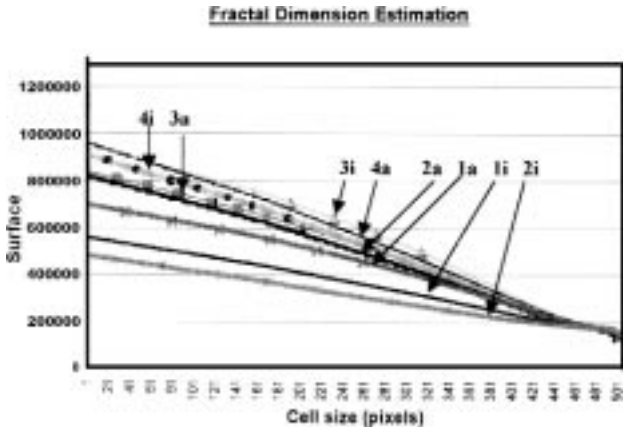

Fig. 5 Representation of the measured surface variation as a function of the cell size for all the samples. The tendency is the same for all the samples whose order in the graphic is 3i, 4a, 4i, 3, 2a, 1a, 1i, and 2i

Table 2 Overall defects in the samples

I.D.	1i	1a	2i	2a	3i	3a	4i	4a
%Defect	0.38	0.91	0.29	2.73	2.60	1.25	5.45	7.30

Table 3 Fractal dimension D_f of the samples

I.D.	1i	1a	2i	2a	3i	3a	4i	4a
D_f	2.592	2.605	2.612	2.712	2.670	2.700	2.750	2.770

and the confidence level of the measurement to be set. To obtain the maximum number of significant data, the interval was taken as unity with a 0.05 confidence level. The average number of steps was 506. In order to demonstrate that the samples exhibited the same behavior and that what varied was the complexity of the microstructure and not the microstructure itself, the program had to analyze and complete all the established steps.

The main objective of the measurement was to find a parameter characteristic of the microstructure of the sample under analysis. This parameter is obtained from the fluorescence density of the previously impregnated samples characterizing the interconnected defects network. It is important to note that samples with a higher degree of overall fluorescence density do not show this because they have accumulated defects (where a lot of resin is concentrated), because their defects network is more complex. To demonstrate this, the amount and distribution of defects were measured by image analysis. This is summarized in Table 2 and Fig. 4.

Figure 4 shows the distribution of the defects as a function of their size. As can be seen, the distribution is very similar in all the samples studied. Though the overall number of defects varies, no important differences in their size distribution can be appreciated. Thus, an image with stronger fluorescence density does not imply the existence of accumulated fluorescence due to larger defects. Therefore, the microstructure is basically the same, but the modification of certain spray parameters develops defect networks with greater complexity.

3.2 Determination of the Connectivity: Fractal Dimension

The penetration of the resin into the coating depends on the size, distribution, and quantity of connections between defects reaching the surface. Therefore, resin's penetration gives information on the network's complexity and the possible effect of the spray conditions.

The next step is to establish whether the structures that are studied using fractal geometry are in fact of a fractal nature. For this, it must be established whether the plot of the measured points shows an asymptote from which a slope can be calculated. The samples showed the behavior represented in Fig. 5. The variation of the surface area versus cell size indicates an important proportionality, which implies that the microstructure of the samples is fractal in nature.

Consequently, the microstructural complexity of the samples can be characterized by the fractal dimension, which is measured by calculating the slope of the linear part of the plot. This value is added to the Euclidean dimension, as indicated in Eq 2, to obtain the fractal dimension. The results are shown in Table 3.

As the fractal dimension is a measurement of the interconnected defects and the complexity of their network, some differences can be observed if compared with the results shown in Table 2, for which only the percentage of defects were calculated. Both results are complementary, because the shape, distribution, and size of the defects, as well as the complexity of their interconnected network, need to be viewed for a better evaluation of the coating microstructure.

3.3 Influence of Spraying Parameters

The penetration of the resin, when the relative velocity of the torch-substrate changes, was evaluated by comparing samples 1 and 2. At the intermediate temperature and for the steel substrate, resin penetration was lower when the relative velocity was low. At the same temperature, the aluminum substrate behavior was different. Both velocities produced coatings in which the resin reached the interface. Consequently, a steel substrate produced coatings with a less complex defect network and with better adhesion.

For the same substrate temperature and for the same coating

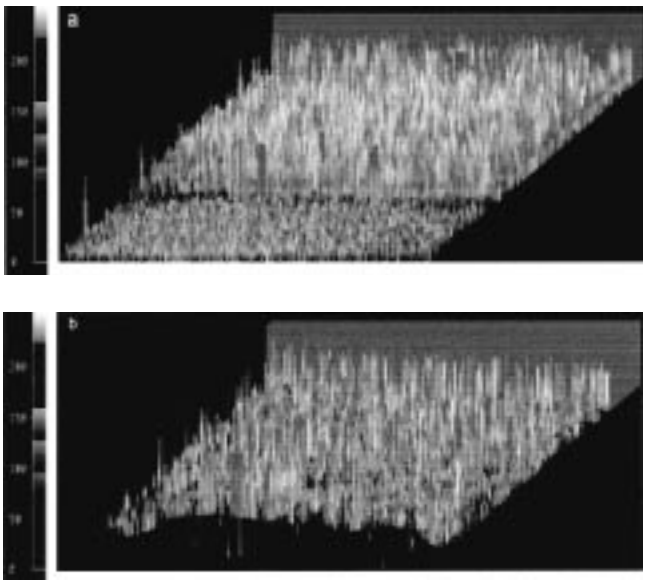

Fig. 6 (**a**) Orthogonal projection of the reconstructed extended focus for sample 2a. The volume under observation is 998.4 × 998.4 × 56.2 μm^3. (**b**) Orthogonal projection of the reconstructed extended focus for sample 1a. The volume under observation is 998.4 × 998.4 × 56.2 μm^3

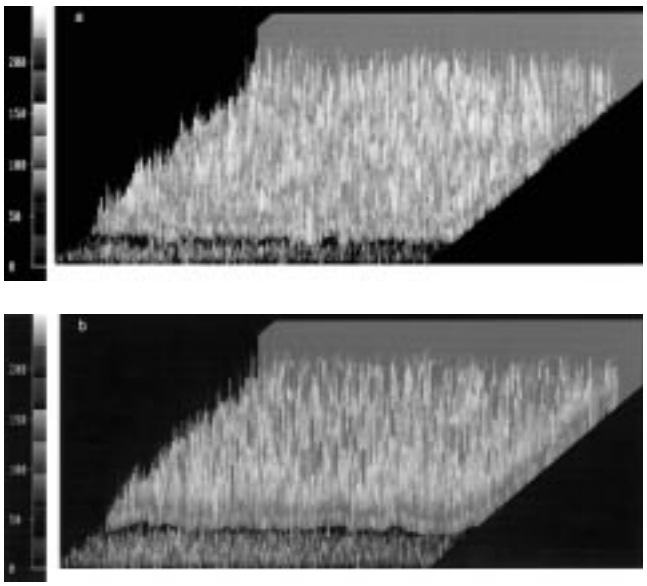

Fig. 7 (**a**) Orthogonal projection of the reconstructed extended focus for sample 3i. The volume under observation is 998.4 × 998.4 × 56.2 μm^3. (**b**) Orthogonal projection of the reconstructed extended focus for sample 3a. The volume under observation is 998.4 × 998.4 × 56.2 μm^3

and substrate pair, the highest relative velocity gave a temperature gradient lower than the one produced when the relative velocity was higher. Consequently, lowering the thermal gradient decreases the formation of vertical cracks of the coating, as can be seen by the comparison of Fig. 6(a) and (b).

Changes in substrate temperature caused marked differences in network complexity. This network is generated by the relaxation of the residual stresses caused by plasma spraying. For low substrate temperatures, the thermal gradient is high, and so residual stresses, which arise from quenching, are increased, and cracks perpendicular to the surface could be formed. For high substrate temperature, quenching stresses decrease because the thermal gradient between the substrate and the arriving particles is lowered. Under these conditions, cracks parallel to the substrate surface generated by the relaxation of thermal stresses increase. The compression strength of the substrate is high, and so, for high coefficient of thermal expansion substrates, the relaxation of these stresses will cause parallel cracking. This is observed for aluminum substrates rather than steel substrates. For the latter, less parallel cracking is seen (Fig. 7a), whereas for aluminum substrates, parallel microcracking is clearly observed (Fig. 7b).

As the fluorescence density and the penetration are higher for high-temperature substrates, it can be concluded that the relaxation of thermal residual stresses is more important and critical for the complexity of the coating microstructure than the relaxation of residual stresses from quenching.

The intermediate temperature is a compromise condition, in which thermal gradients are low enough to reduce quenching stresses during spraying, and, simultaneously, the substrate is not heated so that it generates major thermal stresses. Consequently, the low penetration of the resin indicates that the defects are less connected.

For low-temperature substrates, some accumulation of fluorescence is observed at the interface between the substrate and the coating. This indicates weak adhesion between the splats and the substrate due to the high thermal gradient between them. On increasing the substrate temperature, stresses of thermal origin also increase, and so weaker adhesion is observed. Adhesion quality seemed to be better when particles reached a high-temperature substrate, which can be explained by the strong adhesion of the particles onto the surface as a consequence of the lower thermal gradient between them. The bonding is very high and the particles cannot relax quenching stresses by cracking, and so the stresses remain in the system as residual stresses. Experimentally, this behavior was observed as a decrease in the degree of quenching stresses relaxed by microcracking on the coatings sprayed over substrates at high temperature.

4. Conclusions

Ceramic plasma sprayed coatings are fractal in nature and, consequently, can be studied using fractal geometry. The fractal dimension D offers a semiquantitative tool for comparative evaluation of the complexity, in terms of connectivity and irregularity, of the defects shown by the studied samples. An algorithm for calculating the fractal dimension is proposed. It is based on the fluorescence density of the resin-impregnated coatings.

The complexity of the coating can be evaluated in terms of spraying conditions. Part of the stresses generated during spraying are relaxed by cracking. As the proposed methodology is based on the network of cracks produced when stresses are relaxed, this is the only part that can be evaluated, but in an important volume of the sample and without interference with it. Residual stresses (unrelaxed stresses) of the coating cannot be evaluated with this method. Therefore, some correlation with mechanical properties needs complementary mechanical tests.

The fractal dimension is then a parameter characteristic of the system. Any modification of the spraying conditions changes the complexity of the microstructure, but does not change the microstructure itself.

Acknowledgments

The authors thank Alex del Giorgio and Susanna Castel (Serveis Científico-Tècnics, University of Barcelona) for their valuable comments. They are also grateful to Esther Vilalta (Department of E.Q. Metallúrgia, University of Barcelona) for her consistent help and to Nicolas Baradel for providing the samples.

References

1. A. Ohmori and Chang-Jiu Li: *Thin Solid Films,* 1991, vol. 201, pp. 241-52.
2. T.R. Kino and T.R. Cole: *Physics Today,* ASM International, Materials Park, OH, 1989, pp. 55-62.
3. *ASM Handbook,* ASM International, Materials Park, OH, 1996, vol. 18, pp. 357-61.
4. C.J. Cogswell and C.J.R. Sheppard: in *Confocal Microscopy,* Academic Press Inc., San Diego, CA, 1990, pp. 213-42.
5. L. Bianchi and N. Llorca-Isern: in *Thermal Spray: Surface Engineering via Applied Research,* C.C. Berndt, ed., ASM International, Materials Park, OH, 2000, pp. 29-36.
6. B. Mandelbrot: *The Fractal Geometry of Nature,* W.H. Freeman and Company, New York, NY, 1993.
7. D.L. Turcotte: *Fractals Chaos Geology Geophysics,* Cambridge University Press, Cambridge, United Kingdom, 1992.
8. P. Caligiuri, M.L. Giger, and M. Farus: *Multifractal Med. Phys.,* 1994, vol. 21 (4).
9. P. Treadway and C.C. Berndt: in *Thermal Spray: Research, Design Applications,* C.C. Berndt and T.F. Bernecki, eds., ASM International, Materials Park, OH, 1993, pp. 513-17.
10. M. Guzmán, M.A. Martín, M. Morán, and M. Reyes: *Estructuras Fractales y sus Aplicaciones,* Ed. Labor, Barcelona, Spain, 1993 (in Spanish).
11. N. Baradel: Ph.D. Thesis, Ecole Nationale Supérieure des Mines de Paris, Paris, 1999 (In French).
12. Llorca-Isern, M. Puig, and M. Español: *J. Thermal Spray Technol.*, 1999, vol. 8, pp. 73-78.